Optics and Lasers in Engineering 100 (2018) 234–238

Contents lists available at ScienceDirect

Optics and Lasers in Engineering

journal homepage: www.elsevier.com/locate/optlaseng

A robust sub-pixel subdivision algorithm for image-type angular displacement measurement

Hai Yu*, Qiuhua Wan, Xinran Lu, Changhai Zhao, Yingcai Du

Changchun Institute of Optics, Fine Mechanics and Physics, Chinese Academy of Sciences, Changchun 130033, People's Republic of China

ARTICLE INFO

OCIS codes:
120.0280 130.6010 120.3930

ABSTRACT

The use of an image detector to receive grating images and measure angle displacement via image processing is a relatively new technique, which yields higher resolution and better precision than the traditional moiré fringe method. To improve the robustness of image-type angle measurement, this paper proposes a robust sub-pixel subdivision algorithm based on the least square method. Firstly, by analyzing the characteristic of grating image, a new subdivision algorithm is established based on the least square method. Secondly, the simulations of robustness are completed to prove the performance in theoretically. Lastly, the proposed algorithm is used in a typical image-type angle sensor to test the performance in real case. By test, the proposed method is shown to be more accurate and with better robust than the traditional algorithm (centroid algorithm). In a typical image-type angle sensor, it successfully achieves a resolution of 0.62″ (21-bit), 2^{13}-fold subdivision resolution, and precision of 12.85″. The results presented here may provide a theoretical and technological foundation for further research on small-size, high-resolution photographic rotary encoders.

1. Introduction

Photoelectrical angle-displacement measurement is a high-resolution, high-precision technology which combines optical, mechanical, and electronic functions. Angle sensors are crucial components of many different instruments [1]. Current angle sensors use index grating and scale grating to form moiré fringe, change the moiré fringe to a photoelectrical signal through the receiving element, and realize angular measurement via microprocessor. Many sensors work very well using moiré fringe: The absolute encoder designed by the Heidenhain Company, for example, can reach 27-bit resolution [2]; a likewise large in size, ultra-high resolution absolute encoder was designed by the Goddard Space Center as an optical pattern recognition and image processing technology [3]; the 25-bit absolute encoder designed by Chinese Chengdu Institute of Optics and electronics performs well [4]; and the high-resolution encoder designed by the Chinese Changchun Institute of Optics, Fine Mechanics and Physics reach 0.01″ resolution [5]. These devices all used large grating. Achieving high-resolution measurement with smaller grating is much more difficult.

The digital imaging process may be better served by image detectors equipped to measure angle displacement [6–11]. Researchers have indeed used image detectors to receive grating images and achieve high resolution angle displacement measurement via image processing; scholars in the U.S. [12,13], Serbia [14], Japan [15], Spain [16], Korea [17], China [18,19] and other countries have made notable achievements regarding image type encoders. There have been few studies on subdivision and compensation methods for image detectors, however.

Image type angle measurement technology is a recent advancement for distinguishing disk reticle images to realize high-resolution and high-precision measurements [20]. The principle is illustrated in Fig. 1.

As light passes through the grating, the grating pattern projects onto the linear image sensors. In the process circuit, grating grooves are distinguished and the angle position measure with the subdivision algorithm. Angle subdivisions can be calculated intuitively by this method as-assisted by digital image processing technology. In a previous study, we achieved 1.24″ resolution and 14.6″ measurement precision with grating diameter of 38 mm.

We found those image noise and lens defocuse are the main factors impacting the subdivision algorithm results. Although digital image filtering can filter some noise, it also causes some angle information to be lost. For these reasons, our primary goal in conducting the present study was to secure a new angle subdivision algorithm with robustness to noise and defocusing.

In this paper, we analyzed the imaging characteristics of grating grooves and established a robust subdivision algorithm based on the least square method accordingly. This algorithm can minimize the influence of image noise and lens defocus effectively; it features accurate recognition ability and strong adaptability. We applied the algorithm in

* Corresponding author.
E-mail address: yuhai5158@163.com (H. Yu).

http://dx.doi.org/10.1016/j.optlaseng.2017.09.006
Received 9 May 2017; Received in revised form 7 August 2017; Accepted 6 September 2017
Available online 14 September 2017
0143-8166/

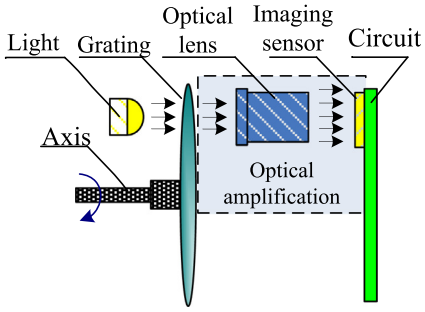

Fig. 1. Angle measurement principle.

an angle sensor and achieved 2^{21} resolution and 12.85″ precision when the grating diameter was 38 mm.

The remainder of this paper is organized as follows. In Section 2, the robust subdivision algorithm is proposed based on the analysis of grating-grooves images. In Section 3, we demonstrate the performance of the algorithm by simulation. Section 4 presents a series of test results. Conclusions are provided in Section 5.

2. Robust subdivision algorithm

Image type angle measurement requires the use of a grating which contains code lines and subdivision reference lines. We inserted reference lines among encoding lines. The code lines are according to shifting coding. The subdivision reference lines are 2^n equal-wide lines distributed uniformly on the circle. Because the lines have a certain width, it is crucial to accurately calculate the center during subdivision. An image of three neighboring subdivision reference lines received by the linear image detector is shown in Fig. 2.

In Fig. 2, the border of a subdivision reference line is not saltatorial and contains three areas: Top, transition, and bottom. The pixels in the top and bottom are relatively stable; the pixels in transition change considerably. The transition and top all include angle information. The traditional calculation method involves the use of a centroid algorithm to calculate the center:

$$R = \frac{\sum_{x\in N} p(x)g(x)}{\sum_{x\in N} p(x)} \tag{1}$$

where N is window size, g(x) are the positions of every pixel in N window, and p(x) are pixel values. This arithmetic can filter noise properly via an average algorithm. The size of N window significantly influences the result of the centroid algorithm. The center position of the image is R_0 and the two subdivision reference lines on either side of the image center are R_1 and R_2, as shown in Fig. 3.

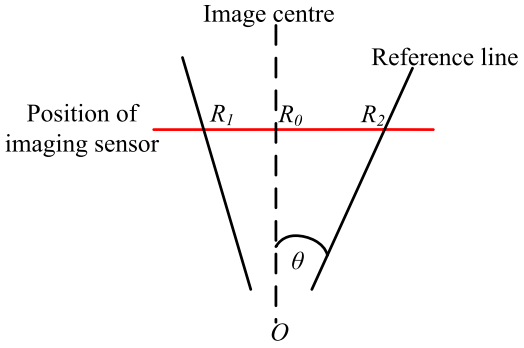

Fig. 3. Calculation with two reference lines.

Set 2^n as the quantity of subdivision reference lines in one circle. When n is sufficiently large (n > 7), $(R_2\text{-}R_0)/(R_2\text{-}R_1)\approx\angle\theta/\angle R_1OR_2$. The measured angle subdivision value can be calculated as follows:

$$\theta = \left|\frac{R_2 - R_0}{R_1 + R_2}\cdot\frac{360^\circ}{2^n}\right| \tag{2}$$

Because the values of R_1 and R_2 are calculated based on the actual window N in Formula (1), this subdivision arithmetic is highly accurate and steady.

We established a new subdivision algorithm to ensure accurate center of reference line information in Formula (2). By analyzing reference lines, we determined a two-fold function is appropriate to fit the image of one reference line. The function is expressed as follows:

$$f(x) = ax^2 + bx + c \tag{3}$$

Where {a, b, c} are coefficients. To fit one subdivision reference line, the difference of squares sum between f(x) and p(x) must reach a minimum in window N:

$$M = \sum_{x\in N}[f(x) - p(x)]^2 \tag{4}$$

To determine whether M is minimal, we calculate partial derivatives of a, b, c, and let the partial derivative be zero:

$$\frac{dM}{da} = 2\sum_{x\in N}[ax^2 + bx + c - p(x)]x^2 = 0 \tag{5}$$

$$\frac{dM}{db} = 2\sum_{x\in N}[ax^2 + bx + c - p(x)]x = 0 \tag{6}$$

$$\frac{dM}{dc} = 2\sum_{x\in N}[ax^2 + bx + c - p(x)] = 0 \tag{7}$$

For easy calculation, Formulas (5–7) can be written as follows:

$$\begin{aligned}&(A_1 - A_3C_1)a + (B_1 - B_3C_1)b = D_1 - D_3C_1\\ &(A_2 - A_3C_2)a + (B_2 - B_3C_2)b = D_2 - D_3C_2\\ &c = D_3 - A_3a - B_3b\end{aligned} \tag{8}$$

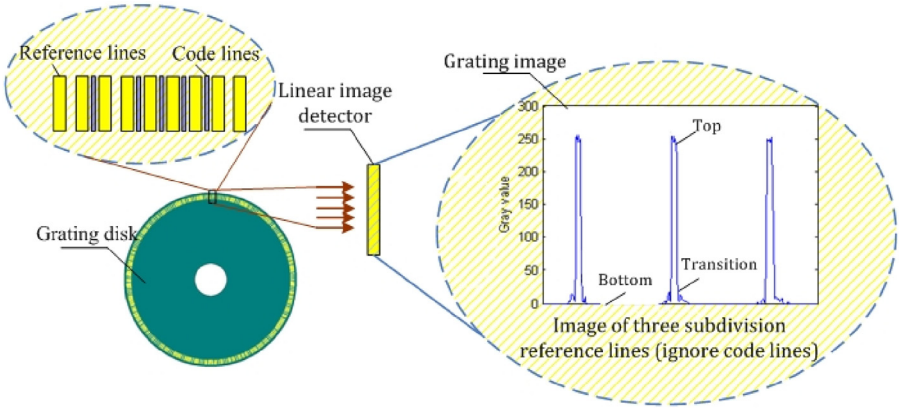

Fig. 2. Image acquisition principle. (The code lines is not considered in this paper).

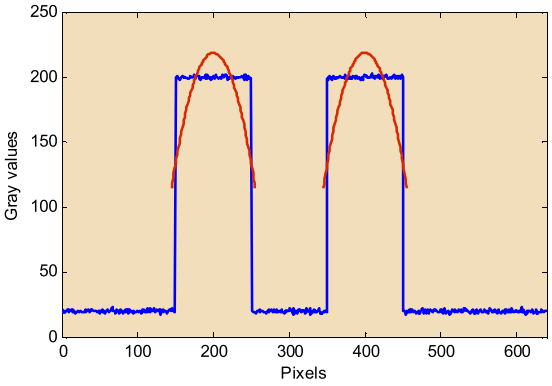

Fig. 4. Anti-noise capability.

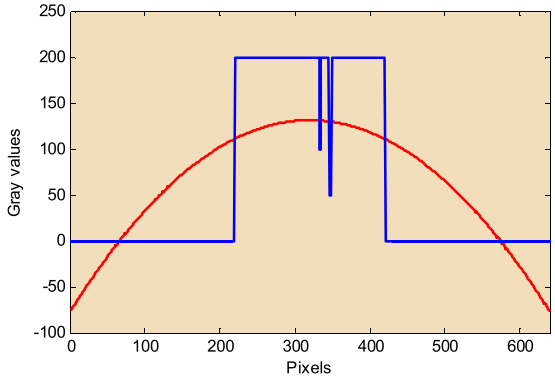

Fig. 5. Calculation result when added dirty-spots.

Table 1
Comparisons of anti-noise capability by θ values.

No.	Method	Non-noise	Noised
1	Centroid algorithm	$60/2^n$	$60.7612/2^n$
	Proposed algorithm	$60/2^n$	$60.7583/2^n$
2	Centroid algorithm	$60/2^n$	$60.7641/2^n$
	Proposed algorithm	$60/2^n$	$60.7570/2^n$
3	Centroid algorithm	$60/2^n$	$60.7622/2^n$
	Proposed algorithm	$60/2^n$	$60.7565/2^n$
4	Centroid algorithm	$60/2^n$	$60.7615/2^n$
	Proposed algorithm	$60/2^n$	$60.7571/2^n$
5	Centroid algorithm	$60/2^n$	$60.7634/2^n$
	Proposed algorithm	$60/2^n$	$60.7578/2^n$

Table 2
Comparison of anti-jamming capability.

No.	Method	Not dirty	Dirty
1	Centroid algorithm	320	319.6245
	Proposed algorithm	320	320.1109
2	Centroid algorithm	320	319.5365
	Proposed algorithm	320	320.1235
3	Centroid algorithm	320	319.6578
	Proposed algorithm	320	320.1324
4	Centroid algorithm	320	319.6367
	Proposed algorithm	320	320.1122
5	Centroid algorithm	320	319.6624
	Proposed algorithm	320	320.1242

where A_1~A_3, B_1~B_3, C_1~C_3, D_1~D_3 are the coefficients of a, b, c. The coefficient matrix is shown as follows:

$$\begin{bmatrix} A_1 & B_1 & C_1 & D_1 \\ A_2 & B_2 & C_2 & D_2 \\ A_3 & B_3 & C_3 & D_3 \end{bmatrix} = \begin{bmatrix} \sum x^4 & \sum x^3 & \sum x^2 & \sum p(x)x^2 \\ \sum x^3 & \sum x^2 & \sum x & \sum p(x)x \\ \sum x^2 & \sum x & 1 & \sum p(x) \end{bmatrix} \tag{9}$$

We can obtain only one group of {*a, b, c*} by calculation.

We let the maximum position of $f(x)$ in window N is the accurate center of one subdivision reference line R. By calculating the derivatives of $f(x)$ and let it be zero, we get the center of one subdivision reference line R as shown in Formula (10):

$$R = -\frac{b}{2a} \tag{10}$$

This algorithm can fit the image of reference lines automatically. Meanwhile, when calculating subdivision values, the comparison reference in Formula (2) always adapts, as robust.

3. Performance analyses

3.1. Anti-noise

We used the matrix function to simulate the image of one ideal subdivision reference line. The range of pixels was set to $x\in\{1\sim640\}$; we set the high gray values to $p(x)=200$ and low gray values to $p(x)=20$. Two center positions of subdivision reference lines are thus 200 and 400. We added Gaussian noise with a mean square of zero and calculated θ with the proposed arithmetic by Formula (1) where $R_0=300$, window N is {135~255} and {335~455}, the results as shown in Fig. 4. We also used the centroid algorithm (Formula (1)) to calculate θ values. We added Gaussian noise for 5 times and the comparison results are shown in Table 1.

As-calculated by the centroid algorithm, the difference in center position between non-added and added noise are all lager than the proposed algorithm. The mean standard deviation of 5-times added is 0.00124, calculated by the centroid algorithm. As-calculated by proposed algorithm, the standard deviation is 0.000709. The fluctuation of proposed algorithm is smaller than centroid algorithm. In other words, our algorithm has stronger robustness to noise than the centroid algorithm.

3.2. Anti-jamming

If the grating disk is stained, the image will be imperfect. In this simulation, the range of pixels was set to $x\in\{1\sim640\}$; when $220\geq x\geq420$, we set the gray values to $p(x)=200$ and when $x\leq220$ or $x\leq420$, we set the gray values to $p(x)=0$. We added some spots on $p(x)$ and recalculated the center with the proposed arithmetic as shown in Fig. 5.

In Fig. 5, the center is 320.1109 as-calculated with the proposed algorithm and 319.6245 per the centroid algorithm. We also did 5-times tests, the results are shown in Table 2. As-calculated by the centroid algorithm, the mean standard deviation of dirty results is 0.051; as-calculated by the centroid algorithm is 0.009. For comparison, the fluctuation of proposed algorithm is even better.

3.3. Anti-defocus

We next applied a Gauss function to simulate a small defocused image. Two neighboring subdivision reference lines are expressed as follows:

$$p_2(x) = Ax^{\frac{-(x-x_1)^2}{2\sigma^2}} + Ax^{\frac{-(x-x_2)^2}{2\sigma^2}} \tag{11}$$

Let $A=200$, $x_1=200$, $x_2=400$, $\sigma=20$. Two center positions of subdivision reference lines are thus 200 and 400, as marked with blue lines in Fig. 6. The set threshold value is 20, so the window areas are {158~242} and {358~442}. We fit two subdivision reference lines by using the proposed algorithm, as marked with red lines in Fig. 6. The center positions were calculated to be $z_1=200$ and $z_2=400$, i.e., were accurate; to this effect, the proposed algorithm has favorable anti-defocus capabilities.

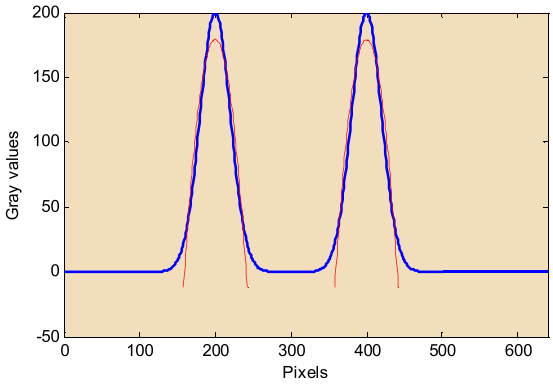

Fig. 6. Small Defocusing simulation. (For interpretation of the references to color in this figure legend, the reader is referred to the web version of this article).

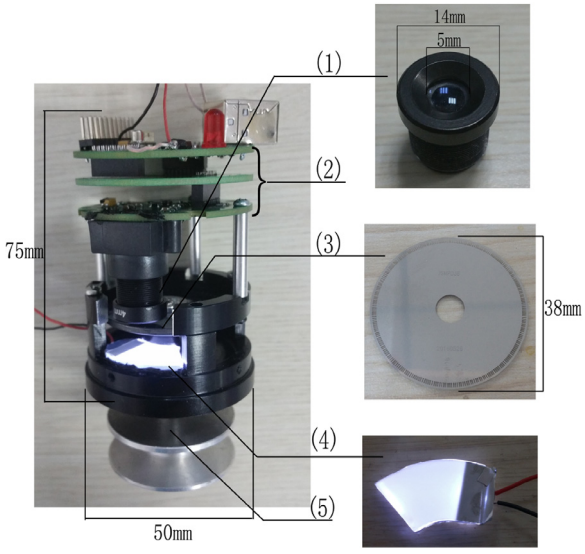

Fig. 7. Experimental image angle sensor: (1) Optical lens, (2) Circuit, (3) Code disc, (4) Light source, (5) Flange.

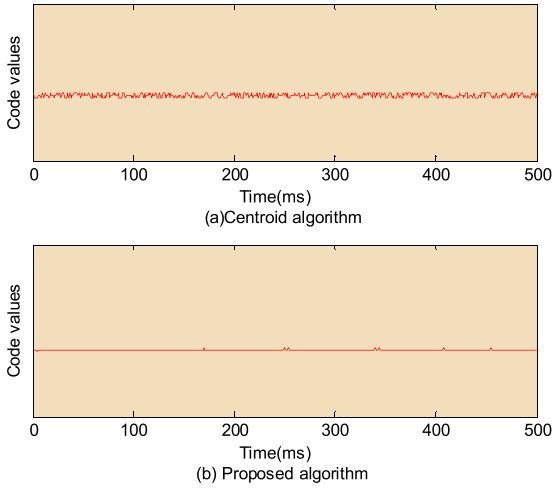

Fig. 8. Wave curve of the output values in static.

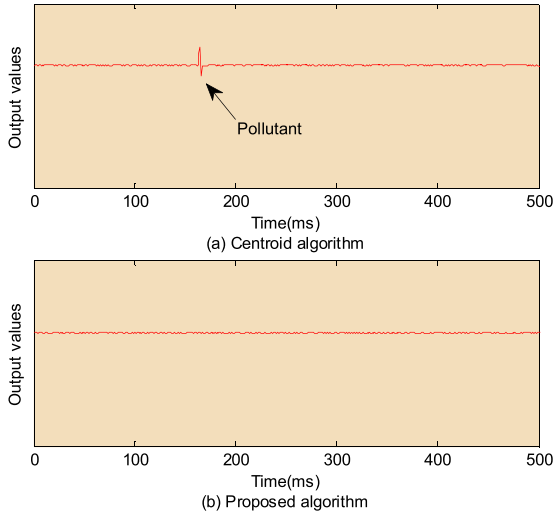

Fig. 9. Wave curve of the output values when polluted.

4. Experiments

We used the robust subdivision algorithm in a typical image type angle sensor to test its performance. The grating diameter was ϕ38 mm, the diameter of the reference line circle was ϕ35 mm, the grating disk had $2^8 = 256$ reference lines, lens magnification was 3.5, and the linear image detector had 640 pixels. The experimental system is shown in Fig. 7.

In present study on image-type angle-measurement, the subdivision algorithm was based on centroid algorithm. So, we do some test by comparing with centroid algorithm, to prove the robustness of the proposed algorithm.

4.1. Robustness test

4.1.1. Anti-noise test

We putted the experimental device on a steady platform and enforced the axis motionless. Set the subdivision be 2^{13}-fold, the quantity of reference lines was 2^8, and the output values have 21-bits data. By the collections of its output numbers, we get the wave curve of the output numbers as shown in Fig. 8.

In Fig. 8(a), when applying the centroid algorithm, the 21st bit was unstable. Inversely, in Fig. 8(b), the proposed robust subdivision algorithm was steady all the 21-bits.

The images had some noises which caused the resolution cannot be more high. In other words, the proposed algorithm outperformed the centroid algorithm in regards to robustness to noise and reliability at higher resolutions.

4.1.2. Anti-jamming test

We let the code disk have small pollutant, and turned the axis in uniform velocity. During the pollutant was in or out of the image detection area, we collected output code numbers, as shown in Fig. 9.

In Fig. 9, when using the proposed algorithm, the output code numbers was not influenced by the pollutant. But when using centroid algorithm, output code numbers were wrong in this area (cannot output by order).

4.1.3. Anti-defocus

When the lens is out of focus, we used the proposed algorithm to test the performance of anti-defocus. By turning the axis slowly, the output numbers can export in right order. This test indicated the output code numbers is not influenced by defocus.

Therefore to sum up, the proposed algorithm is more robust.

4.2. Precision test

We tested for measurement errors by using a 24-bit high precision photoelectrical encoder with precision of 2″. The error was recorded at

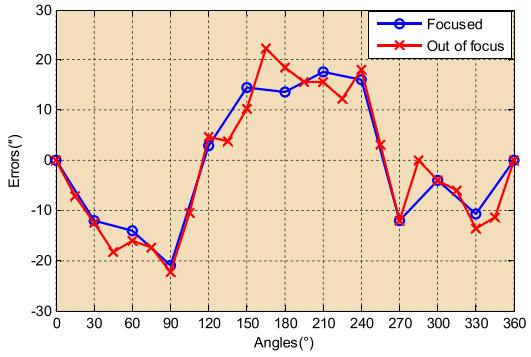

Fig. 10. Errors between focused and out of focus.

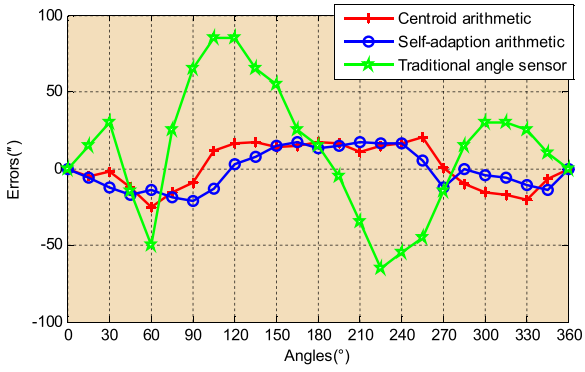

Fig. 11. Detection results. (For interpretation of the references to color in this figure legend, the reader is referred to the web version of this article).

15° intervals during the test. The comparison between focused and out of focus are shown in Fig. 10.

In Fig. 10, the mean-square deviation of focused was 12.85″ and was 13.14 when it was out of focus. The difference of two precision is small. This suggests that the proposed algorithm was influenced by defocus small.

After that, the comparison between centroid algorithm and traditional angle sensor is shown in Fig. 11. Where, the mean-square deviation of the error was 12.85″. The error of the centroid algorithm is marked with a red line (14.3″ mean-square deviation); the error of a traditional angle sensor with moiré fringe is marked with a green line (41.53″ mean-square deviation).

Our results show that the precision of the proposed robust subdivision algorithm is better than that of the traditional angle sensor. The error curve is also steadier than that of the centroid algorithm, suggesting that the proposed algorithm has better measurement precision, because of its robustness.

5. Conclusions

This paper proposed a new angle subdivision algorithm for small-size, high-resolution, high-precision angle displacement measurement via linear image detector. The proposed subdivision algorithm exhibited strong robustness to noise and defocusing, and can achieve 2^{13}-fold subdivision with 12.85″ precision. The results presented here may represent a theoretical and technological foundation for small-size, high-resolution photographic rotary encoders.

Acknowledgment

This project was supported by the National Natural Science Foundation of China (Grant No. 51605465).

References

[1] Hane K, Endo T, Ishimori M, Sasaki M. Integration of grating-image-type encoder using Si micromachining. Sens Actuators A 2002;97–98:139–46.
[2] Kao C-F, Huang H-L, Lu S-H. Optical encoder based on fractional-Talbot effect using two-dimensional phase grating. Opt Commun 2010;283:1950–5.
[3] Mancini D, Cascone E, Schipani P. Galileo high-resolution encoder system. Proc SPIE 1997;3112:328–34.
[4] Tianjin T, Xiangqun C, Bin L. Developing current situation and the trend of photo-electric- angular encoder. Opt Instrements 2005;27:91–5, in Chinese.
[5] Jingwu X, Qiuhua W. 23 bit photoelectric rotary encoder. Opt Machinery 1990;2:52–60, in Chinese.
[6] Luo W, Zhang Y, Feizi A, Gorocs Z, Ozcan A. Pixel super-resolution using wavelength scanning. Light Sci Appl 2016;5:e16060.
[7] Qin J, Silver RM, Barnes BM, Zhou H, Dixson RG, Henn M-A. Deep subwavelength nanometric image reconstruction using Fourier domain optical normalization. Light Sci Appl 2016;5:e16038.
[8] Witte S, Tenner VT, Noom DWE, Eikema KSE. Lensless diffractive imaging with ultra-broadband table-top sources: from infrared to extreme-ultraviolet wavelengths. Light Sci Appl 2014;3:e163.
[9] Cadarso VJ, Chosson S, Sidler K, Hersch RD, Brugger J. High-resolution 1Dmoire´s as counterfeit security features. Light Sci Appl 2013;2:e86.
[10] Sobieranski AC, Inci F, Tekin HC, Yuksekkaya M, Comunello E, Cobra D, et al. Portable lensless wide-field microscopy imaging platform based on digital in-line holography and multi-frame pixel super-resolution. Light Sci Appl 2015;5:e346.
[11] Bianco V, Memmolo P, Paturzo M, Finizio A, Javidi B, Ferraro P. Quasi noise-free digital holography. Light Sci Appl 2016;5:e16142.
[12] Leviton DB, Frey BJ. Ultra-high resolution, absolute position sensors for cryostatic applications. Proc SPIE 2003;4850:776–87.
[13] Leviton DB, Garza MS. Recent advances and applications for NASA's new, ultra-high sensitivity, absolute, optical pattern recog-nition encoders. Proc SPIE 2000;4091:375–84.
[14] Bajić JS, Stupar DZ, Dakić BM, Živanov MB, Nagy LF. An absolute rotary position sensor based on cylindrical coordinate color space transformation [J]. Sens Actuators A 2014;213:27–34.
[15] Sugiyam Y, Matsu Y, Toyod H, Mukozaka N, Ihori A, Abe T, et al. A 3.2 kHz 14-bit optical absolute rotary encoder with a CMOS profile sensor. IEEE Sens J 2008;8:1430–6.
[16] Tresanchez M, Pallejà T, Teixidó M, Palacín J. Using the image acquisition capabilities of the optical mouse sensor to build an absolute rotary encoder. Sens Actuators A 2010;157:161–7.
[17] Kim J-A, Kim JW, Kang C-S, Jin J, Eom TB. Absolute angle measurement using a phase-encoded binary graduated disk. Measurement 2016;80:288–93.
[18] Wang Y-N, Yaun B, Ni X-X. Subdivision technique of absolute angular encoder using array detector. J Chin Zhejiang Univ (Eng Sci) 2011;45:370–4, in Chinese.
[19] Lili Q. Angle-measurement technology of an optical pattern rotary encoder and its hardware implementation. Acta Opt Sin 2013;33:0412001, in Chinese.
[20] Yu H, Wan QH, Lu XR, Du YC, Yang SW. Small-size, high-resolution angular displacement measurement technology based on an imaging detector. Appl Opt 2017;56:755–60.